MnFe<inf>2</inf>O<inf>4</inf> Nanoparticles-Catalyzed C3-Alkylation of Indoles with Benzyl Alcohols under Solvent-Free Conditions

ChemistrySelect

Research Article
doi.org/10.1002/slct.202402007

Chemistry Europe
European Chemical Societies Publishing

www.chemistryselect.org

$MnFe_2O_4$ Nanoparticles-Catalyzed C3-Alkylation of Indoles with Benzyl Alcohols under Solvent-Free Conditions

Ha V. Le,[a, b] Huy X. Le,[a, b] Vy T. B. Nguyen,[a, b] Tu T. Le,[a, b] Hanh N. Nguyen,[a, b] Thuong T. H. Nguyen,[a, b] Tung T. Nguyen,[a, b] Phuoc H. Ho,*[c] Khoa D. Nguyen,[a, b] and Dat P. Tran*[a, b]

Herein, we present an efficient, one-pot reaction for accessing 3-benzylated indoles *via* the coupling of benzyl alcohols with indoles under heterogeneous catalysis by manganese ferrite ($MnFe_2O_4$) nanoparticles. Notably, this reaction, for the first time, employs $MnFe_2O_4$ nanoparticles prepared using a simple grinding method. The high compatibility of $MnFe_2O_4$ nanoparticles enables a broad substrate scope and high regioselectivity. Moreover, this approach offers several attractive highlights including the use of a recyclable oxide catalyst and green and cost-effective alkylating reagents under solvent-free conditions.

Introduction

Indole-based skeletons are one of the most widely investigated heteroaromatic compounds over the past century due to their prevalence as a critical and valuable nucleus in natural products, drug candidates, agrochemicals, and advanced organic materials.[1,2] For instance, 3-substituted indole derivatives have presented in various biologically active molecules, such as anticancer or antitumor agents, leukotriene D4 receptor antagonists, or inhibitors (Figure 1).[3–8] Despite remarkable advances in the functionalization of indole, there remains an imperative need for the development of a sustainable and efficient synthetic procedure for such derivation. The classical strategy for indole alkylation is mostly based on Friedel-Crafts reaction or radical alkylation under harsh reaction conditions.[9,10] However, the regioselectivity of these reactions is strongly controlled by the nature of initial substrates and the inherent properties of the substituent.[11–13] Importantly, competing reactions such as indole polymerization and *N*-alkylation are inevitable, resulting in the formation of regio-isomeric products and a limited substrate scope. These drawbacks lower the atom economy of the applied protocol and increase costs for the isolation and purification of the desired product.[14–16]

The past few decades have witnessed significant progress in the dehydrogenative coupling of carbon-carbon and carbon-heteroatom (C–X) bonds (X=N, O, S).[10,17] Alcohols have emerged as prominent building blocks in C–C bond formation, replacing traditional alkylating reagents due to their non-toxicity, sustainability, and wide availability in diverse structures. In this process, alcohols undergo hydrogen abstraction to generate a carbonyl compound, followed by nucleophilic addition to form double-bond intermediates and *in situ* hydrogenation to yield target products.[18] Complexes of noble metals, such as Ru, In, and Pd coordinated with toxic and intricate organic ligands, have been widely used in most of the alcohol-mediated functionalization at the C3-indole position.[19–23] Alternatively, earth-abundant 3 d transition-metal catalysts including Ni, Fe, Co, Mn, and Cu in pincer complexes, have also exhibited promising catalytic performances on the selective C(sp^2)-H alkylation of indole derivatives, offering more cost-efficient approaches (Figure 2a).[11,24–27] Rueping and co-workers pioneered a solvent-switched regioselective *N*- and C3-benzylation of indolines using manganese complex catalysts.[28] Other manganese pincer complexes have been developed to catalyze the dehydrogenative construction of C3-alkylated indoles and bis(indolyl)methanes.[29,30] Recently, the selective C3-alkenylation of the indole moiety with 2-arylethanol was reported.[31] Despite considerable achievements in this transformation, there have been no reported efforts in the literature to obtain C3-alkylated indoles from alcohols using heterogeneous Mn-based catalysts. Such catalysts can offer undeniable advantages in terms of recyclability, cost reduction, and waste prevention.

Manganese ferrite ($MnFe_2O_4$) nanoparticles, with a spinel structure, have received great attention in the field of functional materials science and technology. Their high magnetic permeability as well as chemical stability and excellent biocompatibility have led to diverse applications of $MnFe_2O_4$ in magnetic

[a] H. V. Le, H. X. Le, V. T. B. Nguyen, T. T. Le, H. N. Nguyen, T. T. H. Nguyen, T. T. Nguyen, K. D. Nguyen, D. P. Tran
Faculty of Chemical Engineering, Ho Chi Minh City University of Technology (HCMUT), 268 Ly Thuong Kiet, District 10, Ho Chi Minh City, Viet Nam 740010
E-mail: tpdat.sdh222@hcmut.edu.vn

[b] H. V. Le, H. X. Le, V. T. B. Nguyen, T. T. Le, H. N. Nguyen, T. T. H. Nguyen, T. T. Nguyen, K. D. Nguyen, D. P. Tran
Vietnam National University Ho Chi Minh City, Linh Trung Ward, Thu Duc City, Ho Chi Minh City, Viet Nam 720400

[c] P. H. Ho
Chemical Engineering, Competence Centre for Catalysis, Chalmers University of Technology, Gothenburg SE-412 96, Sweden
E-mail: phuoc@chalmers.de

Supporting information for this article is available on the WWW under https://doi.org/10.1002/slct.202402007

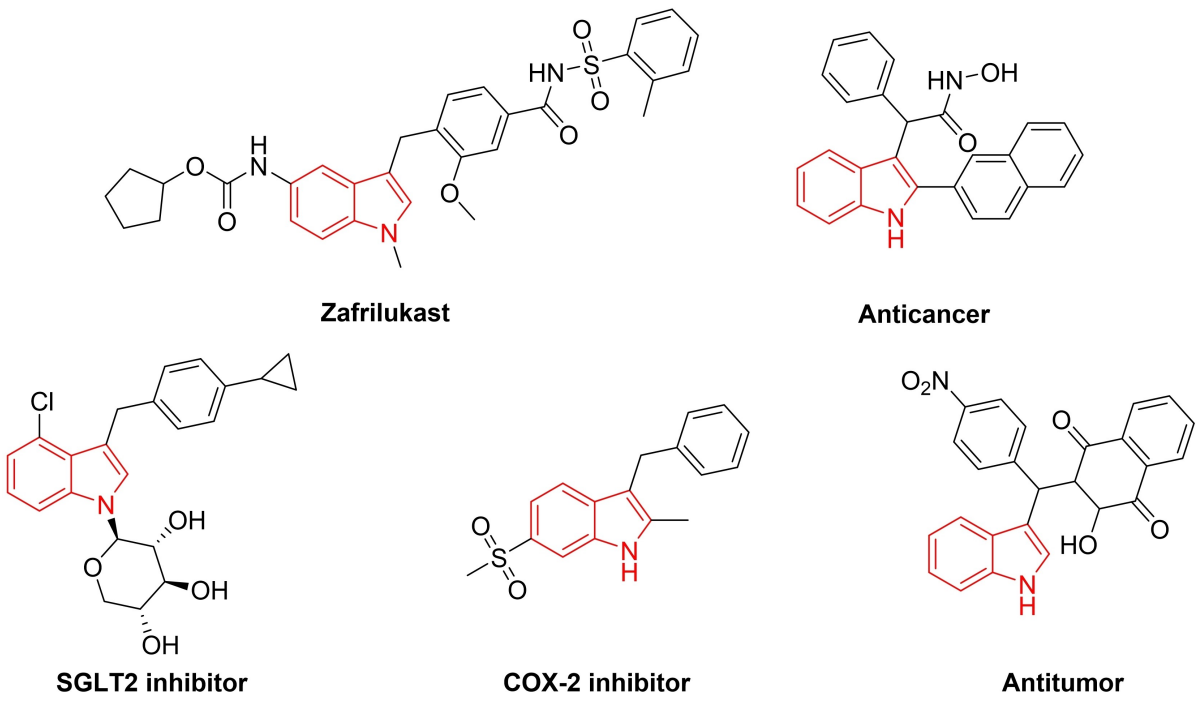

Figure 1. Biologically active relevant skeletons containing a 3-benzylindole scaffold.

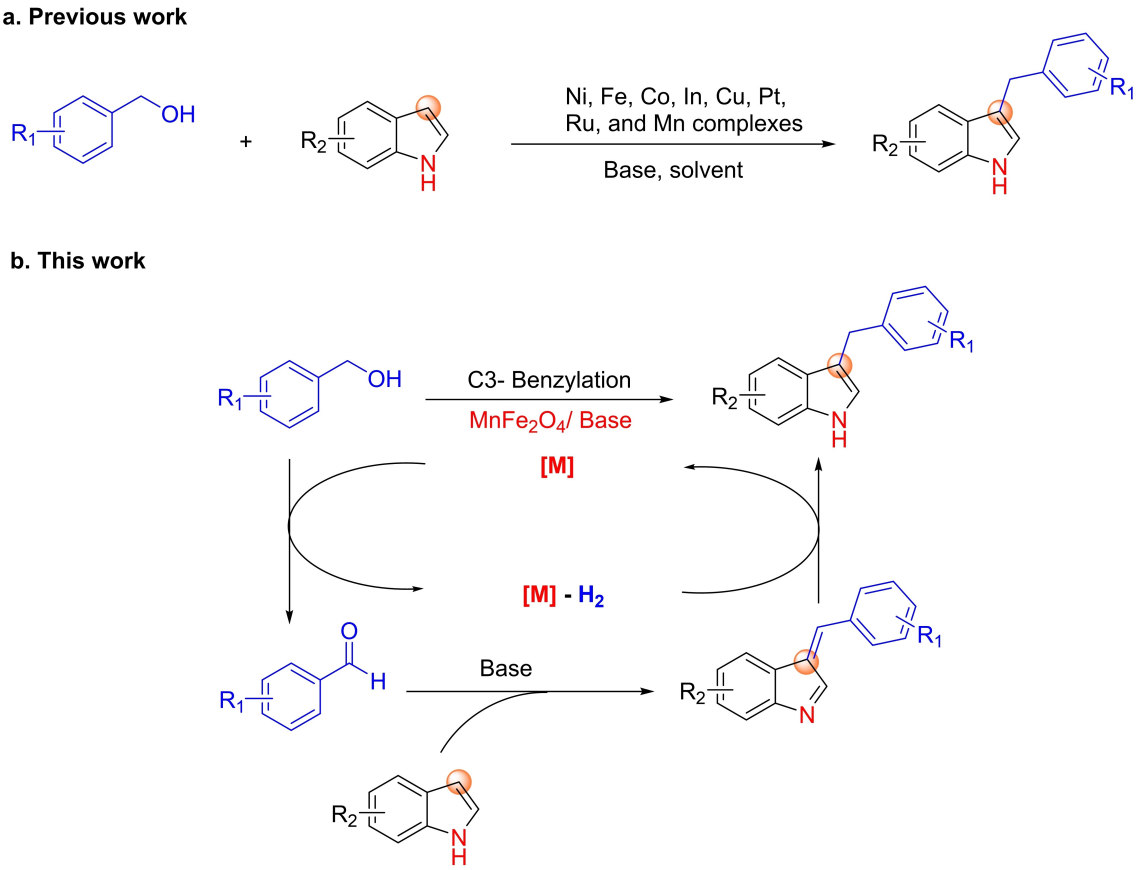

Figure 2. Schematic representation of the selective C3-benzylation of indole *via* catalytic dehydrogenative pathways.

resonance imaging, energy storage, water treatment, and drug delivery.[32–35] Notably, the $MnFe_2O_4$ material has emerged as a potential candidate for heterogeneous catalysis in organic synthesis. Spiro compounds known for outstanding bioactivities

have been successfully synthesized in the presence of $MnFe_2O_4$-based catalysts.[35–37] Continuing our previous efforts towards organic transformation under greener conditions, herein we present a study on the selective C3-alkylation of indole with benzyl alcohol catalyzed by recyclable $MnFe_2O_4$ nanoparticles, which were facilely synthesized via a solid-state reaction (Figure 2b). This work aims to provide a selective and convenient pathway for accessing C3-benzylated indoles under heterogeneous catalysis.

Experimental

Chemicals

All the reagents and metal precursors were purchased from Sigma-Aldrich and were used as received without any further purification.

Preparation of $MnFe_2O_4$

In a typical procedure, $Mn(CH_3COO)_2.4H_2O$ (0.980 g, 4.0 mmol), $Fe(NO_3)_3.9H_2O$ (3.232 g, 8.0 mmol), and polyvinylpyrrolidone (PVP, 2.500 g) were thoroughly ground in a ceramic mortar for 10 min. The resulting mixture was treated with NaOH (1.280 g, 32.0 mmol) and further ground for an additional 30 min before being washed with water until neutralization. The resulting dark brown precipitate obtained *via* centrifugation was dried at 105 °C for 12 h and underwent another grinding stage for 5 min. Subsequently, the ground material was calcined under static air at 550 °C with a temperature ramp rate of 2 °C min^{-1} for 4 h. The obtained solid was denoted as $MnFe_2O_4$-550, where 550 stands for the applied calcination temperature of 550 °C. Additionally, three samples with different annealing temperatures (350, 450, and 650 °C) were also prepared.

Characterization of $MnFe_2O_4$

The crystalline structure of $MnFe_2O_4$ was investigated using a D8 Advance X-ray diffractometer (Bruker, Germany) with a Ni-filter CuK_α radiation. The X-ray diffraction (XRD) measurement was conducted in a 2θ range from 10 to 80° with a step size of 0.04°. Peak position and full width at the half maximum were taken from multiple-fitting mode using OriginPro software, while the crystalline size was calculated by the Scherrer Equation (1).

$$\tau = \frac{0.9\lambda}{\beta\cos\theta} \quad (1)$$

Where λ (nm) is the X-ray wavelength, β (rad) is the full width at half maximum of each peak, and θ (rad) is the Bragg angle.

Morphology of the catalysts was observed by transmission electron microscopy (TEM) on a JEOL 1200 EX2 instrument (Hitachi, Japan). Textural properties of the material were determined by isothermal nitrogen physisorption at 77 K using a Tristar 3000 device (Micromeritics, United States). The sample was outgassed at 150 °C for 16 h prior to the measurement.

Thermogravimetric analysis (TGA) was carried out using an SDT Q600 Thermal Gravimetric Analyzer (TA Instruments, United States). For the measurement, approximately 10 mg of sample was placed in an alumina pan, and then the temperature was increased from 30–800 °C at a heating rate of 5 °C/min in the air atmosphere.

Catalytic Tests

In a typical experiment, indole (58.6 mg, 0.5 mmol), benzyl alcohol (270.4 mg, 2.5 mmol), potassium hydroxide (22.4 mg, 0.4 mmol), and $MnFe_2O_4$-550 (10 mg) were sequentially added into a pressurized 8 mL vial. The reaction was performed at 140 °C under vigorous stirring using a ChemGlass magnetic hot plate stirrer (OptiChem, United Arab Emirates) for 24 h. Upon completion, the reaction mixture was cooled to room temperature, and dibenzyl ether (99.1 mg, 0.5 mmol) was subsequently added as an internal standard. After that, ethyl acetate (2.0 mL) was added dropwise into the reaction vial, followed by vigorous stirring to disperse the internal standard. An aliquot of the resulting mixture was withdrawn and quenched with brine (2.0 mL). The organic phase was then extracted and dried over anhydrous Na_2SO_4 before being analyzed by GC to determine the yield of the benzylation reaction.

Gas chromatographic (GC) analyses were carried out using a GC 2010-Plus device (Shimadzu, Japan) equipped with a flame ionization detector (FID) and an SPB-5 column (length = 30 m, inner diameter = 0.25 mm, and film thickness = 0.25 μm). In the GC system, the oven was held at 160 °C for 1 min, then heated to 280 °C at 40 °C/min, and finally maintained at this temperature for 6 min. Both inlet and detector temperatures were set constant at 280 °C. The GC yield was calculated using dibenzyl ether as the internal standard.

Gas chromatography-mass spectrometry (GC-MS) analyses were conducted on a GCMS-QP2010 Ultra system (Shimadzu, Japan) containing a ZB-5MS column (length = 30 m, inner diameter = 0.25 mm, and film thickness = 0.25 μm). In the GC-MS system, the oven was held at 50 °C for 2 min; heated to 280 °C at 10 °C/min, and maintained at this temperature for 10 min.

The inlet temperature was set constant at 280 °C. MS spectra were compared with the spectra obtained from the NIST library.

The nuclear magnetic resonance spectra (^{1}H-NMR and ^{13}C-NMR) were recorded on an AV 500 spectrometer (Bruker, Germany) using residual solvent peak as a reference.

Results and Discussion

Catalyst Characterization

The grinding method was employed to prepare $MnFe_2O_4$ due to its simplicity and efficiency.[38] Upon addition of NaOH to the well-ground mixture of metal precursors and PVP, a color change from red-orange to dark brown was observed, indicating the formation of $MnFe_2O_4$ precursor in the solid mixture (Figure 3, in the experimental section). PVP utilized as an additive to prevent agglomeration during the preparation process, can be removed *via* the high-temperature treatment in the presence of oxygen.[39,40] Previous studies have reported that the calcination step significantly influences the structure and morphology of obtained materials.[33] Therefore, in this study, the calcination temperature was varied from 350 to 650 °C, yielding a series of $MnFe_2O_4$ samples. TEM images depict the particle sizes and morphology of these samples (Figure 4). Large clusters including nanoparticles with irregular shapes and sizes were observed on the samples calcined (350 and 450 °C) (Figures 4a and b), attributed to a low level of the surface dehydration of the oxides at such temperatures. $MnFe_2O_4$

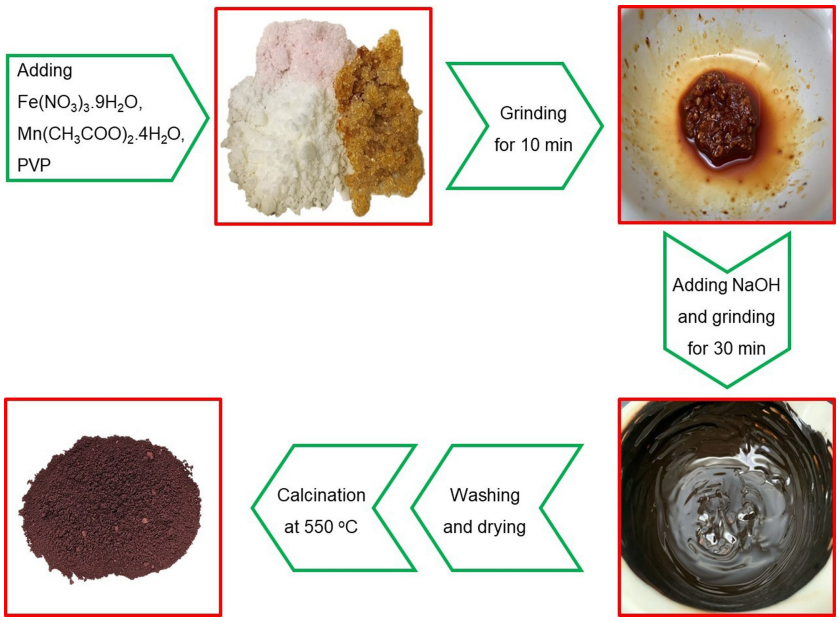

Figure 3. Schematic procedure for the synthesis of $MnFe_2O_4$-550.

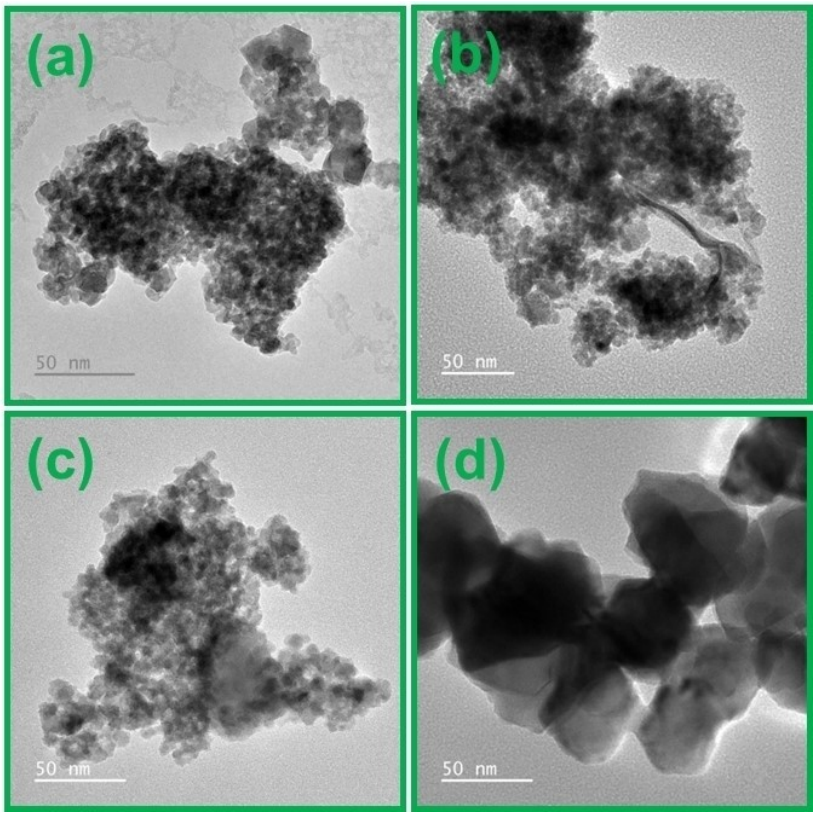

Figure 4. TEM images of $MnFe_2O_4$-350 (a), $MnFe_2O_4$-450 (b), $MnFe_2O_4$-550 (c), and $MnFe_2O_4$-650 (d).

nanoparticles with well-defined shapes were generated when the samples were calcined at 550 and 650 °C (Figure 4c and d). However, due to the sintering effect and electrostatics magnetic attraction, elevating the calcination temperature resulted in the particle size enlargement, for example, from 10–15 nm at 550 °C to 40–50 nm at 650 °C. Such a calcination temperature-dependent tendency was observed for other spinel ferrites, such as $NiFe_2O_4$ and $CoFe_2O_4$, as reported elsewhere.[41–43]

The XRD results of as-synthesized $MnFe_2O_4$ are illustrated in Figure 5a. It was observed that the crystalline $MnFe_2O_4$ phase

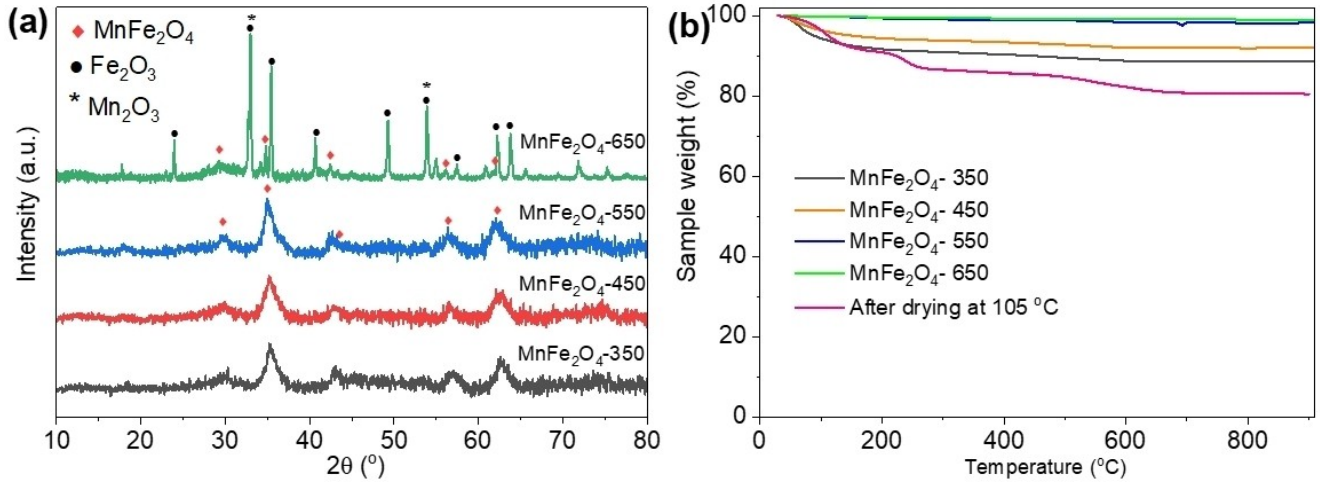

Figure 5. XRD patterns (a) and TGA profiles (b) of the $MnFe_2O_4$ samples.

could be formed at a low calcination temperature of 350 °C. Diffraction peaks at $2\theta = 29.8$, 35.0, 42.8, 56.4, and 62.36° can be assigned to (220), (311), (400), (511), and (440) planes of spinel $MnFe_2O_4$, respectively (JCPDS card no. 10–0319).[44] No diffraction peaks of produced impurities (e.g., manganese oxides and/or ferrite oxides) were detected for these samples. Furthermore, an increase in the calcination temperature to 450 and 550 °C showed a gradual enhancement in peak intensity and a decrease in peak width, indicating higher crystallinity and sintering of the $MnFe_2O_4$ nanoparticles.[45–47] Indeed, the average crystalline size of $MnFe_2O_4$ was increased from 4.4 to 6.5 nm (using Debye-Scherrer's equation), which was consistent with TEM data. Notably, calcination at 650 °C led to the formation of mixed α-Fe_2O_3 and Mn_2O_3 phases due to further oxidation of Mn^{2+} to Mn^{3+}, and this oxidation process partially destabilized the spinel structure of $MnFe_2O_4$.[48–50] These individual phases tended to sinter into large clusters as observed from TEM images. Previous studies have found that $MnFe_2O_4$ remains stable up to 600 °C; beyond this temperature, its conversion to single oxides was observed.[48,51–53]

For the uncalcined $MnFe_2O_4$ sample, the TGA curve showed a 10% weight loss at the temperature range from 70 to 200 °C, which was assigned to the release of adsorbed water in the material (Figure 5b). Further heating the sample to 300 °C led to another weight loss of approx. 5% probably due to the combustion of PVP species which remained after the washing step.[46] Notably, another 5% weight loss was observed in the temperature range from 450 to 650 °C, which can be attributed to the crystal development *via* the thermal condensation of the metal hydroxides. Therefore, the TGA analyses for the $MnFe_2O_4$ samples calcined at 350 and 450 °C also revealed minor weight losses due to the hydroxide dehydration which was not detected for the samples treated at higher temperatures (550–650 °C).

Nitrogen physisorption measurements were performed to investigate the textural properties of the obtained $MnFe_2O_4$ samples (Figure 6a). According to the IUPAC system, the

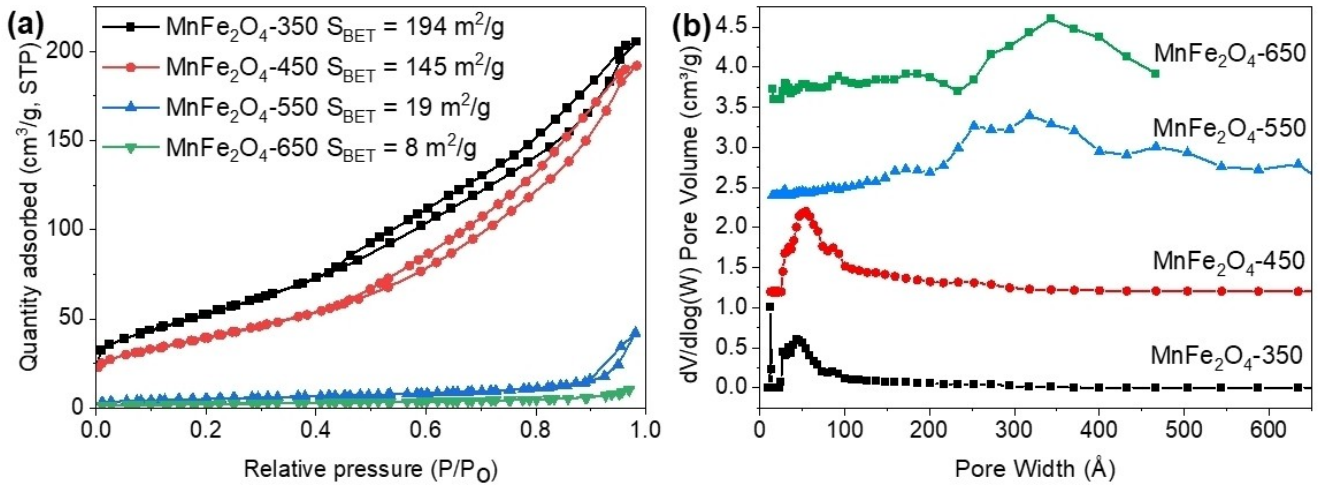

Figure 6. N_2 sorption isotherms (a) and pore size distribution results (b) of the $MnFe_2O_4$ samples.

sorption isotherms of $MnFe_2O_4$-350 and $MnFe_2O_4$-450 were shown in type IV characteristics with an H3 hysteresis loop, indicating the presence of pores with various sizes in the ferrite oxide.[54] Manganese ferrite materials are usually reported to have a low surface area due to their high density.[55–58] However, it has been also reported that the porosity of manganese ferrites can be adjusted upon different synthetic methods and calcination conditions.[55,59] As observed in the TEM images, at low-temperature calcination, for example, 350 or 450 °C, the unwashed PVP species were combusted while the growth of the crystalline phase was insignificant, resulting in the formation of micro- and meso-channels between neighboring nanoparticles (Figure 6b). Consequently, high surface areas (145–194 m^2/g) were obtained for these samples. Increasing the calcination temperatures to 550 and 650 °C caused an increase in the crystal size of the metal oxide and a partial collapse of such channels, thus rapidly decreasing the material surface area to approx. 19 and 8 m^2/g.[44,55]

Catalytic Studies

The as-synthesized $MnFe_2O_4$ nanoparticles were employed as a solid catalyst for the C3-benzylation of indole under a basic medium. First, unsubstituted indole (**1a**) and benzyl alcohol (**2a**) were chosen as model substrates for screening the C3-benzylation conditions (Figure 7). The preliminary studies were performed by heating a reaction mixture of **1a** (0.5 mmol) and **2a** (5.0 equiv.) at 140 °C for 24 h in the presence of KOH (0.2 equiv.) and varied amounts of $MnFe_2O_4$-550 (Table 1). In the absence of $MnFe_2O_4$, only a negligible yield of the desired product **3aa** (4%) was observed, whereas, in the presence of 5.0 mg of $MnFe_2O_4$-550, the yield of C3-benzylated indole was 28% (Entries 1–2). This highlighted the catalytic role of $MnFe_2O_4$ in the reaction. Notably, a complete benzylation selectivity to the C3 position was obtained as none of *N*-benzyl indole and other benzylated derivatives were detected in the resulting mixture. Increasing the catalyst amount to 10 mg improved the product yield to 37%; however, using more than 10 mg of $MnFe_2O_4$ did not improve further the product yield of the coupling reaction (Entries 3–5). Notably, a base must be involved for the C3-benzylation of indole; otherwise, no conversion to the product **3aa** was observed (Entry 6), consistent with the literature.[26,28–30] Moreover, the reaction yield was significantly enhanced with increasing KOH amount. Indeed, the C3-benzylated indole was obtained in a quantitative yield in the reaction using 0.8 equiv. of KOH (Entries 7–10).

Table 1. Effect of catalyst amount, base type, and base amount on the yield of **3aa** (3-benzyl-1H-indole).

Entry[a]	Catalyst amount (mg)	Base	Base amount (equiv.)	GC Yield (%)
1	-	KOH	0.2	4.0
2	5	KOH	0.2	27.6
3	10	KOH	0.2	38.2
4	15	KOH	0.2	38.7
5	20	KOH	0.2	38.0
6	10	-	-	0
7	10	KOH	0.4	70.1
8	10	KOH	0.6	87.9
9	10	KOH	0.8	98.4
10	10	KOH	1.0	98.7
11	10	*t*-BuOK	0.8	81.5
12	10	NaOH	0.8	37.0
13	10	CsOH	0.8	20.0
14	10	*t*-BuONa	0.8	28.0
15	10	*t*-BuOLi	0.8	11.0
16	10	K_2CO_3	0.8	9.1
17	10	K_3PO_4	0.8	7.2
18	10	DBU[b]	0.8	3.6
19	10	DABCO[c]	0.8	2.8

[a] Reaction conditions: indole (0.5 mmol), benzyl alcohol (5 equiv.), $MnFe_2O_4$-550, 140 °C, 24 h. [b] DBU: 1,8-diazabicyclo[5.4.0]undec-7-ene. [c] DABCO: 1,4-diazabicyclo[2.2.2]octane.

Next, various organic and inorganic bases were applied for the reaction. The alkaline hydroxides and *tert*-butoxides were found to be efficient for the reaction but with different performances. Good-to-excellent yields of **3aa** were observed, for example, 81 and 98% in the presence of *t*-BuOK and KOH (Entries 9 and 11), respectively, while using strong bases of other alkali ions such as NaOH, CsOH, *t*-BuONa, *t*-BuOLi produced considerably lower yields of **3aa** in the range of 11–37% (Entries 12–15). Basic inorganic salts (K_2CO_3, K_3PO_4) and amines (DBU, DABCO) failed to afford the desired product with poor yields recorded (< 10%) (Entries 16–19). These results suggested that the C3-benzylation depends on both the base strength and the involved alkali ion.[21,30,31] Similar to previous

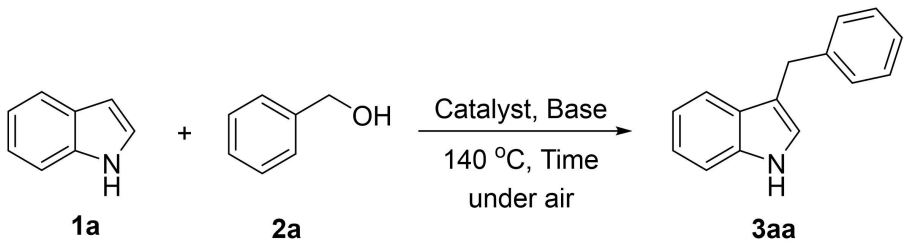

Figure 7. Model reaction between indole and benzyl alcohol for screening the reaction conditions.

studies on the C3-benzylation of indole using molecular catalysts, adding strong polar solvents including glycerol, DMSO, DMF, and H_2O to the reaction mixture immediately stopped the desired transformation while moderate yields (53–55%) were observed in the reaction using non-polar solvents such as toluene and DCB (Table 2, Entries 1–6).[28,60] In the absence of an additional solvent, benzyl alcohol might play a dual role as a reagent and a medium for the reaction, affording the best yield of 98% (Entry 7).[26,60]

The reaction temperature had a notable impact on the C3-benzylation of indole. The desired product was not detected at temperatures below 80 °C and only low yields of **3aa** (<40%) were achieved in the temperature range from 100 to 130 °C under identical conditions (Entries 8–13). However, the reaction was significantly accelerated upon increasing the temperature 140 °C, readily producing **3aa** in an excellent yield of 98% after 24 h (Entry 7). It is evident that the hydrogen transfer between the heterogeneous metal sites and the substrates in a basic medium would be more favorable at an elevated temperature.[18,60] Interestingly, expanding the reaction time to 30 h caused a considerable yield loss of 12% for **3aa** (Entries 14–19). It is hypothesized that 3-benzylidene-3H-indole, which was considered as an intermediate after nucleophile addition, could further react with another indole molecule to form bis(indolyl)methanes.[30] Pazur and co-workers also suggested that a prolonged heating process accelerated the bis-addition of the desired product, leading to a decrease in the yield of the C3-benzylated indole.[61]

Table 2. Effect of solvent, reaction temperature, and reaction time on the yield of **3aa** (3-benzyl-1H-indole).

Entry[a]	Solvent	Temperature (°C)	Time (h)	GC Yield (%)
1	Glycerol	140	24	0
2	H_2O	140	24	0
3	DMF[b]	140	24	0
4	DMSO[c]	140	24	0
5	DCB[d]	140	24	57.0
6	Toluene	140	24	59.6
7	-	140	24	98.4
8	-	30	24	0
9	-	60	24	0
10	-	80	24	0
11	-	100	24	10.5
12	-	120	24	18.1
13	-	130	24	35.0
14	-	140	2.5	12.1
15	-	140	5	32.0
16	-	140	10	61.0
17	-	140	15	80.4
18	-	140	20	90.0
19	-	140	30	86.4

[a] Reaction conditions: indole (0.5 mmol), benzyl alcohol (5 equiv.), $MnFe_2O_4$-550 (10 mg), KOH (0.8 equiv.). [b] DMF: *N,N*-dimethylformamide. [c] DMSO: dimethyl sulfoxide. [d] DCB: 1,4-dichlorobenzene.

The catalytic activity of the $MnFe_2O_4$ samples, prepared through calcination at different temperatures ranging from 350 to 650 °C was evaluated for the KOH-assisted reaction of indole with benzyl alcohol at 140 °C for 24 h (Figure 8). Excellent yields of **3aa** were observed for most of the $MnFe_2O_4$ samples except $MnFe_2O_4$-350. The reaction catalyzed by this material only gave a lower yield of 65% possibly due to the abundance of the hydroxyl groups on the $MnFe_2O_4$ surface, consistent with a weight loss of approximately 3.0 wt% in the temperature zone from 350 to 800 °C of the TGA profile of this catalyst. These hydroxyl groups may hinder the interaction of the substrate molecules with the metal sites. Considering the similar catalytic performances of other manganese ferrites, it can be concluded that the particle size as well as the crystalline phase of the ferrite had generally a negligible impact on the reaction. Both the single oxides, namely iron and manganese oxides, were found to be responsible for the C3-benzylation of indole, providing the desired product in good yields (50–70%). However, the synergistic effect of the Fe and Mn sites in the $MnFe_2O_4$ catalyst significantly enhanced the transformation to a quantitative yield of **3aa** (Figure 8). For comparison purposes, the catalytic tests of other spinel ferrites including $CoFe_2O_4$ and $NiFe_2O_4$ were also performed. Importantly, the cooperation of manganese and iron metals showed the best catalytic performance.

Since the selective benzylation of indole with benzyl alcohol using the $MnFe_2O_4$ catalyst was performed in the liquid phase, the possibility of metal leaching should be carefully considered. In certain cases, the unstable active sites of solid catalysts could be dissolved and thus migrate into the reaction phase.[62,63] Such leached metal species could catalyze the reaction *via* a homogeneous mechanism, mainly contributing to the recorded activity. Therefore, in this study, a leaching test for the $MnFe_2O_4$-catalyzed transformation was carried out. Initially, the reaction of indole with benzyl alcohol was performed under the standard conditions in the presence of 10 mg of $MnFe_2O_4$-550 for 10 h, resulting in a **3aa** yield of approx. 60%. Subsequently, the $MnFe_2O_4$ catalyst was removed by filtration. The collected liquid phase was transferred into a new pressurized vial and heated to 140 °C for another 14 h. The further formation of **3aa**, if any, was monitored by GC at the predetermined time intervals. After 3 h, a slight increase in the **3aa** yield to approx. 64% was observed, possibly due to the unreacted intermediate species. However, this yield remained almost unchanged afterward, indicating that the catalysis was indeed heterogeneous (Figure 9a). Any migrating species, if present, made a negligible contribution to this conversion.

The utilization of solid catalytic systems for organic reactions can simplify the purification process, reduce synthetic expenses, and mitigate environmental problems associated with metal-based wastes. On the other hand, the efficient and facile reusability of solid catalysts is one of the grand benefits of heterogeneous catalysis.[64,65] To discover this advantage, the $MnFe_2O_4$ catalyst was separated from the reaction medium by simple filtration. Prior to its subsequent use under identical

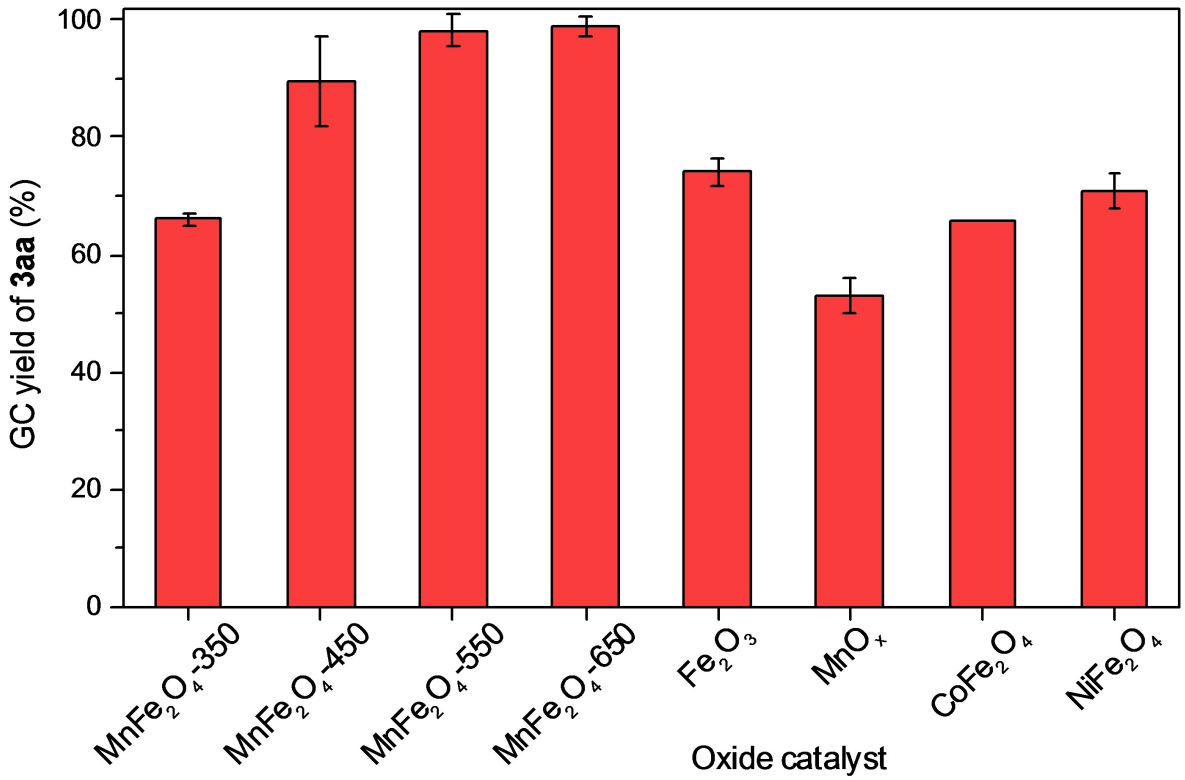

Figure 8. Effect of oxide catalyst type on the product yield. Reaction conditions: Catalyst (10 mg), indole (0.5 mmol), benzyl alcohol (5 equiv.), KOH (0.8 equiv.), 140 °C, 24 h.

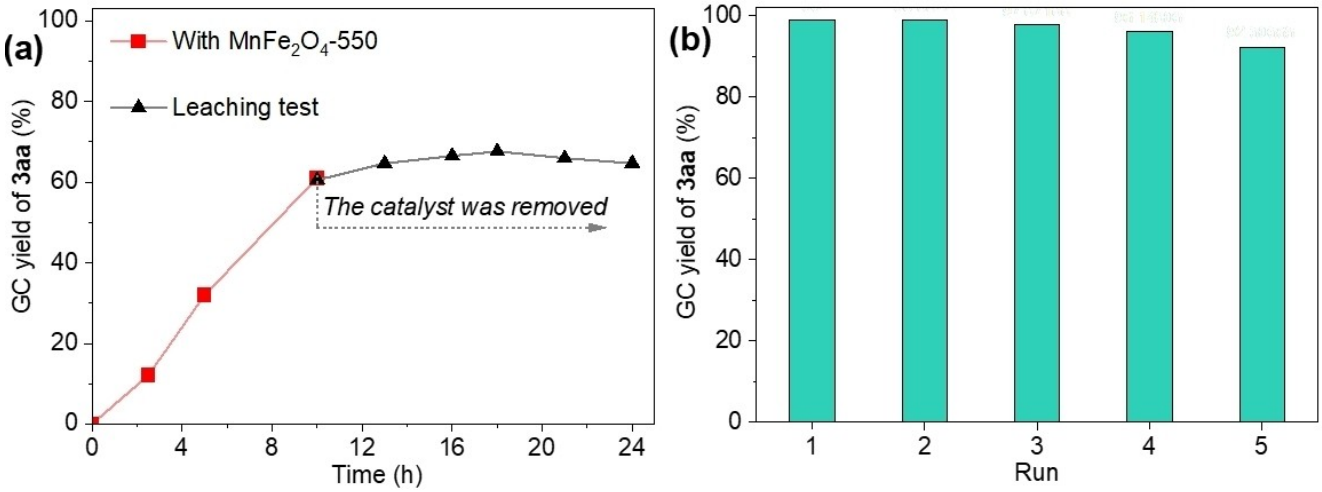

Figure 9. Leaching test (a) and recycling study (b).

conditions, the catalyst underwent washing with an excess amount of ethyl acetate and acetone, followed by drying at 105 °C for 12 h. Remarkably, only a minor decrease in the yield of the target product was recorded in the fifth run, indicating the excellent performance of the regenerated catalyst for this protocol (Figure 9b).

With the optimized reaction conditions established, the scope of substrates was examined. A wide range of indoles was initially investigated with the coupling of benzyl alcohol **2a** (Figure 10). An isolated yield of 81% was obtained for **3aa**. In general, indoles bearing electron-donating groups such as 5-methoxyindole and 5-benzyloxyindole smoothly reacted with benzyl alcohol, yielding the corresponding products in good-to-excellent isolated yields (**3ba, 3ca**). Indoles with 5-substitution of halogen exhibited a slower reaction rate but still afforded the desired products in decent yields (**3da–3fa**, 54–70%), except for 5-chloroindole (**3ga**, 88%). No coupling products were detected in the coupling of 5-nitro- and 5-cyanoindole with benzyl alcohol, indicating that strong electron-withdrawing substituents could inhibit the reaction. However, no clear trends

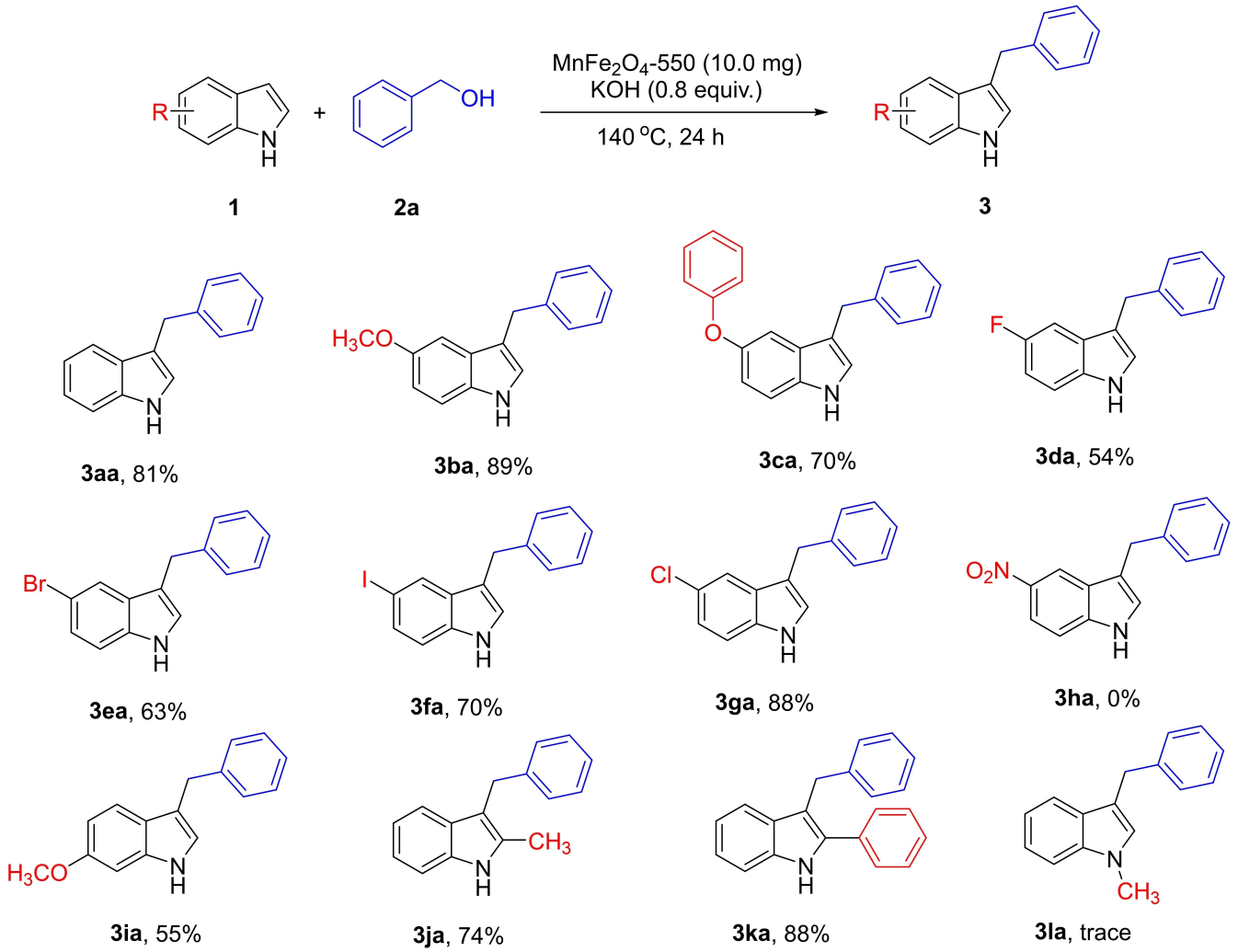

Figure 10. Isolated yield of the C3-benzylated indoles produced from the reaction of substituted indoles with benzyl alcohol.

in the reactivity were observed for other substituted indoles. For example, despite the electron-donating effect on the indole molecule, the methoxy group at the C6 position lowered the reaction yield to 55% (**3ia**), as compared to the case of unfunctionalized indole. By contrast, the C3-benzylation of 2-methylindole or 2-phenylindole proceeded efficiently with **2a**, yielding the products **3ja** and **3ka**, respectively, in good yields. These synthetic results also indicated that the steric hindrance at the 2-position had no significant impact on the catalytic alkylation at the C3 position of indole, which can encourage the construction of further complicated compounds *via* this transformation. Similar to previous publications, *N*-methylindole failed to furnish the C3-benzylated products, which could be explained by the involvement of the N–H bond in the formation of intermediate anion under a basic environment.[25,30,66]

Next, further investigation into substituted benzyl alcohols was conducted (Figure 11). Electron-rich 2-methylbenzyl and 4-methylbenzyl alcohol smoothly converted to corresponding products **3ab** and **3ac** in good yields (87%). It was pleased that a quantitative yield of **3ad** was achieved for 3-methylbenzyl alcohol. Notably, the presence of 2-chloro group in benzyl alcohol diminished the yield of coupling product (**3ae**, 35%) possibly due to the steric effect. However, chloro-substituted benzyl alcohols at the *para* and *meta* positions were well tolerated under the applied conditions, affording the corresponding alkylated indole products **3af** and **3ag** in good yields (80–87%). Electron-poor benzyl alcohol, for example, 3-(trifluoromethyl)benzyl alcohol furnished a moderate yield (57%) of target product **3ah**. It has been reported that electron-withdrawing groups suppressed the stability of benzylic intermediates, thus deactivating benzyl alcohol molecules in Lewis or Brønsted acid-catalyzed Friedel-Crafts reaction.[25,67] On the other hand, our catalyst was ineffective in activating heteroaromatic alcohols such as 2-thiophene methanol or 2-pyridine methanol.

Conclusions

In summary, we have established a practical and highly efficient procedure to accommodate value-added 3-benzylindoles through the use of corresponding indoles and benzyl alcohols.

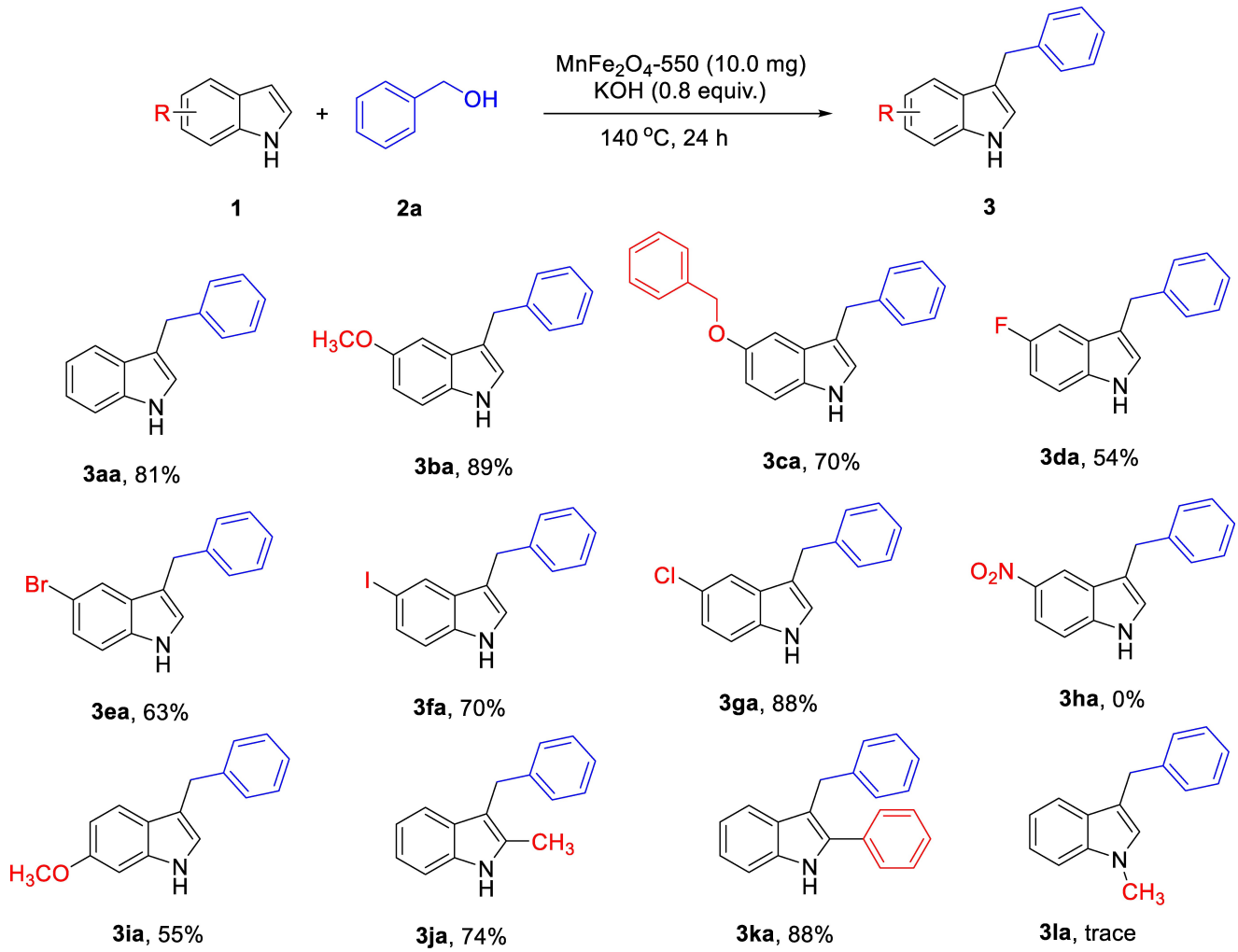

Figure 11. Isolated yield of the C3-benzylated indoles produced from the reaction of indole with substituted benzyl alcohols.

The findings remark the first application of easily synthesized manganese ferrite nanoparticles has been operated as a heterogeneous catalyst for this transformation. The regioselective C3-benzylated products were achieved in good to excellent yields (up to 99%). Such high yields of products without catalyst leaching make the use of $MnFe_2O_4$ promising because the catalyst was easily separated from the products which is the greatest advantage of using heterogeneous catalysts compared to their homogeneous counterparts. Our future work will focus on gaining further insight into the mechanism and expanding the scope to include secondary benzyl alcohols and aliphatic alcohols. We believe that this methodology could pave the way for the construction of medicinal compounds and sustainable synthetic pathways.

Supporting Information Summary

Synthetic procedure, ^{1}H- and ^{13}C-NMR results of the obtained products.

Acknowledgements

We acknowledge Ho Chi Minh City University of Technology (HCMUT), VNU-HCM for supporting this study.

Conflict of Interests

The authors declare no conflict of interest.

Data Availability Statement

The data that support the findings of this study are available from the corresponding author upon reasonable request.

Keywords: $MnFe_2O_4$ · C3-alkylation · Indole · Benzyl alcohol · Heterogeneous catalysis

[1] R. B. Van Order, H. G. Lindwall, *Chem. Rev.* **1942**, *30*, 69–96.

[2] J. A. Leitch, Y. Bhonoah, C. G. Frost, *ACS Catal.* **2017**, *7*, 5618–5627.
[3] J. C. McKew, F. Lovering, J. D. Clark, J. Bemis, Y. Xiang, M. Shen, W. Zhang, J. C. Alvarez, D. Joseph-McCarthy, *Bioorg. Med. Chem. Lett.* **2003**, *13*, 4501–4504.
[4] R. T. Jacobs, P. R. Bernstein, L. A. Cronk, E. P. Vacek, L. F. Newcomb, D. Aharony, C. K. Buckner, E. J. Kusner, *J. Med. Chem.* **1994**, *37*, 1282–1297.
[5] C.-H. Yao, J.-S. Song, C.-T. Chen, T.-K. Yeh, M.-S. Hung, C.-C. Chang, Y.-W. Liu, M.-C. Yuan, C.-J. Hsieh, C.-Y. Huang, M.-H. Wang, C.-H. Chiu, T.-C. Hsieh, S.-H. Wu, W.-C. Hsiao, K.-F. Chu, C.-H. Tsai, Y.-S. Chao, J.-C. Lee, *J. Med. Chem.* **2011**, *54*, 166–178.
[6] H. Lu, G. Zhu, T. Tang, Z. Ma, Q. Chen, Z. Chen, *iScience* **2019**, *22*, 214–228.
[7] C. Zhang, Y. Qu, B. Niu, *Biorg. Med. Chem.* **2016**, *24*, 5781–5786.
[8] S. Kathiravan, T. Zhang, I. A. Nicholls, *RSC Adv.* **2023**, *13*, 11291–11295.
[9] S.-L. Liu, R. Zhao, M. Li, H. Yang, L. Zhou, S. Fang, *Org. Lett.* **2023**, *25*, 1375–1379.
[10] S.-L. Liu, H. Liang, H. Yang, L. Gao, L. Zhou, S. Fang, M.-P. Song, *ChemistrySelect* **2020**, *5*, 12819–12822.
[11] Kamal, M. Khatua, S. Rani, B. Goswami, S. Samanta, *J. Org. Chem.* **2023**, *88*, 5827–5843.
[12] D. F. Taber, P. K. Tirunahari, *Tetrahedron* **2011**, *67*, 7195–7210.
[13] G. Casnati, M. Francioni, A. Guareschi, A. Pochini, *Tetrahedron Lett.* **1969**, *10*, 2485–2487.
[14] X. Zhu, A. Ganesan, *J. Org. Chem.* **2002**, *67*, 2705–2708.
[15] K.-S. Yeung, M. E. Farkas, Z. Qiu, Z. Yang, *Tetrahedron Lett.* **2002**, *43*, 5793–5795.
[16] O. Ottoni, A. d. V. F. Neder, A. K. B. Dias, R. P. A. Cruz, L. B. Aquino, *Org. Lett.* **2001**, *3*, 1005–1007.
[17] L. Zhang, R. Zhao, C. Liu, Z. Li, J.-L. Niu, H.-R. Yang, L. Gao, S.-L. Liu, L. Zhou, *Adv. Synth. Catal.* **2023**, *365*, 3461–3466.
[18] A. Porcheddu, G. Chelucci, *Chem. Rec.* **2019**, *19*, 2398–2435.
[19] L. Wu, R. Jiang, J.-M. Yang, S.-Y. Wang, S.-J. Ji, *RSC Adv.* **2013**, *3*, 5459–5464.
[20] A. E. Putra, K. Takigawa, H. Tanaka, Y. Ito, Y. Oe, T. Ohta, *Eur. J. Org. Chem.* **2013**, *2013*, 6344–6354.
[21] N. Biswas, R. Sharma, D. Srimani, *Adv. Synth. Catal.* **2020**, *362*, 2902–2910.
[22] R. A. Jagtap, B. Punji, *Asian J. Org. Chem.* **2020**, *9*, 326–342.
[23] A. K. Guin, S. Pal, S. Chakraborty, S. Chakraborty, N. D. Paul, *J. Org. Chem.* **2023**, *88*, 16755–16772.
[24] M. Hu, Y. Jiang, N. Sun, B. Hu, Z. Shen, X. Hu, L. Jin, *New J. Chem.* **2021**, *45*, 10057–10062.
[25] G. Di Gregorio, M. Mari, F. Bartoccini, G. Piersanti, *J. Org. Chem.* **2017**, *82*, 8769–8775.
[26] N.-K. Nguyen, D. H. Nam, B. V. Phuc, V. H. Nguyen, Q. T. Trinh, T. Q. Hung, T. T. Dang, *Mol. Catal.* **2021**, *505*, 111462.
[27] Y. Wang, M. Wang, Y. Li, Q. Liu, *Chem.* **2021**, *7*, 1180–1223.
[28] J. C. Borghs, V. Zubar, L. M. Azofra, J. Sklyaruk, M. Rueping, *Org. Lett.* **2020**, *22*, 4222–4227.
[29] V. Yadav, E. Balaraman, S. B. Mhaske, *Adv. Synth. Catal.* **2021**, *363*, 4430–4439.
[30] A. Mondal, R. Sharma, B. Dutta, D. Pal, D. Srimani, *J. Org. Chem.* **2022**, *87*, 3989–4000.
[31] M. Zhao, X. Li, X. Zhang, Z. Shao, *Chem. Asian. J.* **2022**, *17*, e202200483.
[32] J. Kalidass, T. Sivasankar, *J. Taiwan Inst. Chem. Eng.* **2023**, *144*, 104766.
[33] N. Akhlaghi, G. Najafpour-Darzi, *J. Ind. Eng. Chem.* **2021**, *103*, 292–304.
[34] Z. Naderi, J. Azizian, *J. Photochem. Photobiol. B: Biol.* **2018**, *185*, 206–214.
[35] A. R. Liandi, A. H. Cahyana, A. J. F. Kusumah, A. Lupitasari, D. N. Alfariza, R. Nuraini, R. W. Sari, F. C. Kusumasari, *Case Stud. Chem. Environ. Eng.* **2023**, *7*, 100303.
[36] R. Ghahremanzadeh, Z. Rashid, A. H. Zarnani, H. Naeimi, *Appl. Catal. A: Gen.* **2013**, *467*, 270–278.
[37] H. Naeimi, Z. Rashid, A. H. Zarnani, R. Ghahremanzadeh, *New J. Chem.* **2014**, *38*, 348–357.
[38] Z. Zhang, G. Yao, X. Zhang, J. Ma, H. Lin, *Ceram Int.* **2015**, *41*, 4523–4530.
[39] G. Ghosh, M. Kanti Naskar, A. Patra, M. Chatterjee, *Opt. Mater.* **2006**, *28*, 1047–1053.
[40] H. Shao, Y. Huang, H. Lee, Y. J. Suh, C. O. Kim, *Curr. Appl. Phys.* **2006**, *6*, e195–e197.
[41] S. Asiri, M. Sertkol, H. Güngüneş, M. Amir, A. Manikandan, İ. Ercan, A. Baykal, *J. Inorg. Organomet. Polym. Mater.* **2018**, *28*, 1587–1597.
[42] Sapna, N. Budhiraja, V. Kumar, S. K. Singh, *J. Supercond. Nov. Magn.* **2018**, *31*, 2647–2654.
[43] K. Maaz, A. Mumtaz, S. K. Hasanain, A. Ceylan, *J. Magn. Magn. Mater.* **2007**, *308*, 289–295.
[44] J. Chen, W. Wen, L. Kong, S. Tian, F. Ding, Y. Xiong, *Ind. Eng. Chem. Res.* **2014**, *53*, 6297–6306.
[45] M. Goodarz Naseri, E. B. Saion, H. A. Ahangar, M. Hashim, A. H. Shaari, *J. Magn. Magn. Mater.* **2011**, *323*, 1745–1749.
[46] P. Ning, C. C. Liu, Y. J. Wang, X. Z. Li, R. Ranjithkumar, Z. H. Gan, Y. Y. Wu, T. Fu, *Ceram Int.* **2020**, *46*, 20105–20115.
[47] S.-L. Kuo, N.-L. Wu, *J. Power Sources* **2006**, *162*, 1437–1443.
[48] Z. Zhang, Y. Wang, Q. Tan, Z. Zhong, F. Su, *J. Colloid. Interface Sci.* **2013**, *398*, 185–192.
[49] C. Simon, A. Blösser, M. Eckardt, H. Kurz, B. Weber, M. Zobel, R. Marschall, *Z Anorg. Allg. Chem.* **2021**, *647*, 2061–2072.
[50] M. A. Gabal, S. S. Ata-Allah, *J. Phys. Chem. Solids* **2004**, *65*, 995–1003.
[51] S. V. Bhandare, R. Kumar, A. V. Anupama, H. K. Choudhary, V. M. Jali, B. Sahoo, *J. Magn. Magn. Mater.* **2017**, *433*, 29–34.
[52] M. Stoia, C. Păcurariu, E.-C. Muntean, *J. Therm. Anal. Calorim.* **2017**, *127*, 155–162.
[53] C. Dong, G. Wang, L. Shi, D. Guo, C. Jiang, D. Xue, *Sci. China Phys. Mech. Astron.* **2013**, *56*, 568–572.
[54] M. Thommes, K. Kaneko, A. V. Neimark, J. P. Olivier, F. Rodriguez-Reinoso, J. Rouquerol, K. S. W. Sing, *Pure Appl. Chem.* **2015**, *87*, 1051–1069.
[55] K. Ashwini, H. Rajanaika, K. S. Anantharaju, H. Nagabhushanad, P. Adinarayana Reddy, K. Shetty, K. R. Vishnu Mahesh, *Mater Today Proc.* **2017**, *4*, 11902–11909.
[56] G. Ramadoss, S. P. Suriyaraj, R. Sivaramakrishnan, A. Pugazhendhi, S. Rajendran, *Sci. Total Environ.* **2021**, *765*, 142707.
[57] T. Lazarova, D. Kovacheva, M. Georgieva, D. Tzankov, G. Tyuliev, I. Spassova, A. Naydenov, *Appl. Surf. Sci.* **2019**, *496*, 143571.
[58] M. A. Iqubal, R. Sharma, S. Jheeta, Kamaluddin, *Life* **2017**, *7*, 15.
[59] H. B. Desai, L. J. Hathiya, H. H. Joshi, A. R. Tanna, *Mater Today Proc.* **2020**, *21*, 1905–1910.
[60] R. Cano, M. Yus, D. J. Ramón, *Tetrahedron Lett.* **2013**, *54*, 3394–3397.
[61] E. J. Pazur, N. R. Tasker, P. Wipf, *Org. Biomol. Chem.* **2023**, *21*, 8651–8657.
[62] M. Hara, K. Nakajima, K. Kamata, *Sci. Technol. Adv. Mater.* **2015**, *16*, 034903.
[63] N. T. S. Phan, C. W. Jones, *J. Mol. Catal. A: Chem.* **2006**, *253*, 123–131.
[64] M. Miceli, P. Frontera, A. Macario, A. Malara, *Catalysts* **2021**, *11*, 591.
[65] H. V. Le, V. B. Nguyen, H. H. Pham, K. D. Nguyen, P. H. Ho, P. Trens, F. Di Renzo, *Catalysts* **2021**, *11*, 1252.
[66] C. Pi, X. Yin, X. Cui, Y. Ma, Y. Wu, *Org. Lett.* **2019**, *21*, 2081–2084.
[67] E. Emer, R. Sinisi, M. G. Capdevila, D. Petruzziello, F. De Vincentiis, P. G. Cozzi, *Eur. J. Org. Chem.* **2011**, *2011*, 647–666.

Manuscript received: April 26, 2024